processes

MDPI

Article

Hydrogen Storage Behavior and Performance of Multiple Cold-Rolled MgH_2/Nb_2O_5 Nanocomposite Powders

M. Sherif El-Eskandarany *, Naser Ali, Fahad Al-Ajmi, Mohammad Banyan and Ahmed A. Al-Duweesh

Nanotechnology and Applications Program, Energy and Building Research Center, Kuwait Institute for Scientific Research, Safat 13109, Kuwait; nmali@kisr.edu.kw (N.A.); ftajmi@kisr.edu.kw (F.A.-A.); mbanyan@kisr.edu.kw (M.B.); aduweesh@kisr.edu.kw (A.A.A.-D.)
* Correspondence: msherif@kisr.edu.kw

Abstract: The global interest in MgH_2 is due to the natural availability of Mg and its capacity to retain hydrogen at a concentration of up to 7.60 wt.%. Despite its appealing characteristics and ease of production on an industrial scale at ambient temperature using the reactive ball milling (RBM) technique, MgH_2 is a highly stable chemical with sluggish hydrogenation and dehydrogenation rates below 300 °C. Among the different methods used to improve the hydrogenation/dehydrogenation kinetic behavior of MgH_2, mechanical treatment and/or catalysis are regarded to be the most effective methods. The purpose of this research was to explore the effectiveness of several cold rolling (CR) stages on the hydrogenation properties of recycled magnesium rods, as well as the effect of the resulting RBM on the final product. For this process, the as-received waste Mg-rods were firstly cold-rolled 200 times and then remilled under H_2 atmosphere for 100 h. The as-RBM powders were then cold-rolled for 100 passes and then ball-milled with 10 and 15 wt.% Nb_2O_5 powders for 50 h. The results showed that when the materials were subjected to different types of defects (dislocations, stacking faults, and twining) generated by CR and RBM, their gas absorption/desorption kinetics were improved. This was indexed by their ability to achieve a long cycle lifetime at lower temperatures when compared with the as-received materials. The powders were further improved in terms of kinetics and decomposition temperature upon RBM with Nb_2O_5 for 50 h. The nanocomposite MgH_2/10 wt.% and 15 wt.% Nb_2O_5 exhibit good hydrogen storage capabilities at a comparatively low temperature (225 °C) with a long cycle life that extended from 110 h to 170 h, without serious degradation in storage capacity and kinetics.

Keywords: hydrogen storage material; lattice imperfections; cold rolling; reactive ball milling; catalyzation; cycle-life-time

Citation: El-Eskandarany, M.S.; Ali, N.; Al-Ajmi, F.; Banyan, M.; Al-Duweesh, A.A. Hydrogen Storage Behavior and Performance of Multiple Cold-Rolled MgH_2/Nb_2O_5 Nanocomposite Powders. *Processes* **2022**, *10*, 1017. https://doi.org/10.3390/pr10051017

Academic Editor: Paola Ammendola

Received: 10 April 2022
Accepted: 17 May 2022
Published: 19 May 2022

1. Introduction

Because of the significant worldwide environmental changes caused by carbon dioxide emissions, and the massive use of finite fossil fuel resources, finding alternative and renewable energy sources is critical for a secure and sustainable future. Concerns regarding combustion engine pollution, as well as other difficulties associated with large-scale mining, transportation, processing, and use of fossil fuels, are growing. [1]. The increased risks posed by global warming as a result of the use of fossil fuels necessitate the adoption of innovative methods to harness the limitless sources of energy [2]. Hydrogen is an energy carrier option that has great potential as a new renewable and clean energy source [3]. It is an efficient, secure, and flexible fuel source that can readily be transformed into the required type of energy while emitting no hazardous pollutants. As a consequence, hydrogen has been selected as the optimal fuel for mobile and stationary applications [4,5].

It is widely expected that hydrogen will become the primary fuel for the majority of cars and portable devices within a few decades for a variety of reasons, the majority of which are related to hydrogen's fascinating and pioneering characteristics, which include

the following: (i) hydrogen is a colorless, odorless, nontoxic, carbon-free gas whose only byproduct is water; (ii) hydrogen is the energy vector that could provide a bridge from the fossil energy economy to the renewable energy economy; and (iii) it can be stored [6]. Notably, when hydrogen gas is burned, the sole emission is water vapor. As a consequence, hydrogen combustion produces no carbon dioxide (CO_2) [7]. Obviously, hydrogen is a less polluting fuel than gasoline since it produces relatively little exhaust emissions. Hydrogen has the potential to outperform an internal combustion engine in terms of fuel cell engine efficiency. The same quantity of hydrogen will propel a fuel cell vehicle at least twice as far as a gasoline-powered vehicle. In comparison to fossil fuels, the potential alternative fuel with its previously stated favorable characteristics also displays attractive properties [5].

Hydrogen storage, which encompasses both hydrogen production and consumption and so plays a critical role in establishing a hydrogen economy [8], has been the subject of much research for many years. Metals and alloys have the ability to absorb hydrogen in its molecular state, therefore functioning as hydrogen sponges. Around 50 metallic elements in the periodic table have variable degrees of hydrogen absorption, resulting in a diverse variety of hydrogen storage materials [9]. Metal hydrides have a higher hydrogen storage density than hydrogen gas (0.99 hydrogen atoms/cm^3) or liquid hydrogen (4.2 hydrogen atoms/cm^3). [10] Thus, metal hydride storage enables the safe and volume-efficient storage of hydrogen for onboard vehicle applications. Magnesium hydride (MgH_2) has been identified as one of the most promising hydrogen storage compounds for use in real-world light automobile applications. This is because magnesium is a light, cheap metal capable of storing up to 7.60 wt.% hydrogen.

Despite these attractive properties, the slow hydrogenation and dehydrogenation rates of MgH_2 pose considerable barriers to its use in fuel cell applications [11]. The kinetics of MgH_2 powder absorption and desorption may be increased by adding catalysts to make the hydrogenation properties fast enough for practical applications [12] or by milling the powders for a prolonged length of time [13]. In fact, prolonged ball milling often boosts the impact of grain boundaries and hydrogen transport [14]. As a result of the introduction of different types of defects, such as lattice and point defects, into the lattice of ball-milled powders, the stable phase of MgH_2 destabilizes [15]. As Floriano et al. have shown, similar flaws may also occur during the cold rolling of magnesium metal [16]. It has been suggested [17,18] that increasing the length of ball milling time lowers powder grain sizes, hence increasing both grain boundaries and active surface area. As a consequence, a more direct path for hydrogen diffusion throughout the bulk area is expected.

Meanwhile, and in addition to the mechanically induced method, doping MgH_2 with catalytic agents has been identified as a realistic scenario used to enhance the slow kinetics of this metal hydride. Since the 1990s, a lengthy list of pure transition metals (TM), such as Ti, Zr, V, Nb, Fe, Co, Ni, and Mn [19–21], as well as their alloys, such as TiV [22], CrTi [23], $TiMn_2$ [24], and $ZrNi_5$ [25], have been developed. Almost all of these reported catalytic agents have resulted in considerable advantages, as measured by reduced hydrogen sorption/desorption temperatures and quicker hydrogenation/dehydrogenation kinetics [2]. In contrast to the extensive list of advantageous long-range order catalysts, El-Eskandarany presented the first research using short-range order material of an amorphous-$Zr_{70}Ni_{20}Pd_{10}$ powder for enhancing MgH_2 [26]. In addition, it has been reported that mechanical treatment of bulk Mg has shown significant improvement of the hydrogenation properties of MgH_2 [27]. It was reported that using such a metastable amorphous phase resulted in a substantial improvement in the kinetics of MgH_2. Table 1 provides some further selected published findings from several categories for MgH_2, as well as MgH_2-based hydrogen storage systems.

Table 1. Selected MgH_2-nanocomposite hydrogen storage systems.

Material	Preparation	Properties	References
MgH_2	As-received	Storage density of up to 7.6 wt.% with slow kinetics and poor thermodynamic characteristics necessitating dehydrogenation temperatures of 300 °C.	[28]
MgH_2	Pure Mg powders were ball-milled under 50 bar (reactive ball milling, RBM) of hydrogen pressure for 200 h	Single, stable phase of β-MgH_2 was obtained upon milling for 25 h. After 200 h of RBM time, the decomposition temperature and activation energy were recorded to be 399 °C and 131 kJ/mol, respectively. The times required for complete absorption and desorption of 7 wt.% of hydrogen at 250 °C were recorded to be 3140 s and 35,207 s under 10 and 0 bar, respectively. Complete 600 absorption/desorption cycles were achieved.	[13]
MgH_2-10 wt.% TM (TM; Fe, Co, Ni, Cu nanoparticles)	Ar atmosphere/high-energy ball milling (HEBM)/4 h	Mg–Fe: Absorption/10 bar/350 °C: 5.1 wt.%/9.1 min, E_a = 86 kJ/mol Mg–Co: Absorption/10 bar/350 °C: 4.3 wt.%/7.7 min, E_a = 75 kJ/mol Mg–Ni: Absorption/10 bar/350 °C: 5 wt.%/6.1 min, Ea = 72 kJ/mol Mg–Cu: Absorption/10 bar/350 °C: 4.6 wt.%/15.3 min, Ea = 76 kJ/mol	[29]
MgH_2-1 at % Zr	H_2-RBM/300 rpm/20 h + annealing at 100 °C/40 bar H_2/24 h	Absorption: 5.5 wt.%/4000 s/300 °C Absorption of nanocomposite: 3.5 wt.% H_2/6000 s/100 °C Dehydrogenation: 5.5 wt.% H_2/2000 s/350 °C	[30]
MgH_2-10 wt.% Mn nanoparticles	H_2-RBM/450 rpm/5 h	Onset desorption temperature: 175 °C and 6.7, 6.5, and 6.1 wt.% hydrogen released within 5, 10, and 25 min at 300, 275, and 250 °C, respectively.	[31]
MgH_2/8 wt.% Nb_2O_5+2 wt.% Ni	Disks of nanocomposite coating with Ni powder (3 layers)	5.5 wt.% hydrogen storage density and fast absorption/desorption kinetics of 2.6/3 min at 250 °C with 400 h life cycle. MgH2-20 wt.% TiO_2	[32]
MgH_2-20 wt.% TiO_2 nanoparticles	H_2-RBM/1 h/8 bar	Absorption/20 bar/350 °C: 3.8 wt.%/2 min Desorption/1 bar/350 °C: 4.4 wt.%/8.5 min	[33]
MgH_2-15 wt.% TiFe	H_2-RBM/450 rpm/5 h	Onset desorption temperature: 175 °C Hydrogen released: 6.5 wt.% H_2/10 min at 300 °C E_a: 72.5 kJ/mol	[34]
MgH_2-40 wt.% TiFeMn	Ar-HEBM/40 h	Absorption/40 bar/80 °C: 4 wt.%/3600 s Desorption/ 3 bar/240 °C: 2.57 wt.%/7200 min	[35]

Aim of the Present Study

As can be realized from the literature, authors employed either high-energy ball milling or cold rolling [36] to improve the hydrogen storage characteristics of the MgH_2 system. The use of reactive ball milling (RBM) in tandem with multistep cold rolling has not yet been reported, to the best of our knowledge. In contrast to the conventional practice of introducing lattice defects into Mg- bulk materials in order to improve their hydrogenation/dehydrogenation conditions through a cold rolling process [27], the present work aimed to investigate the synergetic effect of high-energy reactive ball milling of plastically deformed cold-rolled Mg flakes on hydrogenation/dehydrogenation as well as decomposition processes. When compared with the cold rolling process, which results in severe plastic deformation of magnesium lattices, high-energy ball milling results in different types of lattice imperfections, such as point and lattice defects, which are introduced through the action of the milling media, whereby the Mg flakes are trapped and nipped between the steel balls. The combination of the two methods may result in better lattice imperfection and significant improvements in the behavior of Mg metal in terms of absorption/desorption kinetics when compared with either approach alone. Secondly, we also investigated the behavior of as-prepared MgH_2 powders, which have been milled for an extended period of time, when subjected to significant plastic deformation caused by the cold rolling procedure. In addition, the impact of doping the cold-rolled MgH_2 milled powders with a common catalytic agent, Nb_2O_5, was investigated as well. Moreover, the current research sought to investigate the impact of cold pressing on the hydrogenation/dehydrogenation kinetics and cyclability of MgH_2.

2. Materials and Methods

Figure 1 displays the experimental procedure of preparing MgH_2 and the mechanical treatment procedure of cold rolling and high-energy ball milling.

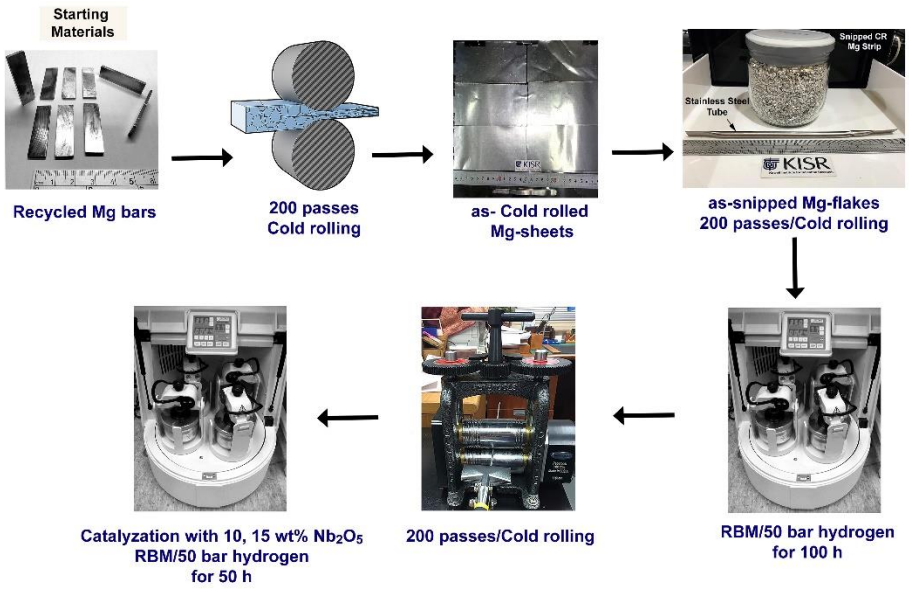

Figure 1. Flowchart diagram illustrating the multipreparation steps used to prepare nanocomposite MgH_2/Nb_2O_5 powders.

2.1. Materials and Sample Preparations

A batch of 30 bars (200 mm in length, 5 mm in diameter) of recycled Mg (99.5 wt.%) chips were acquired from Shanghai Xinglu Chemical Technology Co. Ltd., Shanghai, China, and utilized as feedstock materials. Niobium pentoxide (Nb_2O_5) powders (99.9 wt.%, 10 μm) purchased from Sigma-Aldrich (Sigma-Aldrich, Inc., St. Louis, MO, USA) were used as catalytic agent at a concentration of 10–20 wt.% to enhance the hydrogen storage behavior of Mg and to improve its hydrogen storage kinetic behavior.

The Mg-rods were snipped into shorter rods (~100 mm in length) and sonicated in a cold acetone solution for 10 min. The rods were then washed with pure ethanol before being dried in an oven at 180 °C for 18 h. This treatment stage was required to eliminate any undesired hydrocarbon impurities from the rod's surfaces. The materials were then cold-rolled (CR) on a typical two-tool steel drum cold roller machine for 50–200 passes. After CR, the snipped strips were cleaned with acetone and ethanol and then dried in an oven at 180 °C overnight. The as-snipped Mg flakes (Figure 1) were charged and sealed within a helium (He) glove box (UNILAB Pro Glove Box Workstation, mBRAUN, Glove Box Workstation UNILAB Pro, Dieselstr, 31, D-85748 Garching, Germany) in a stainless steel (SUS304) tube (8 cm diameter and 200 mm length). The tube containing Mg flakes was severely CR for a variety of passes (50 to 200 passes) using the manual cold roller.

The as-CR tube system was opened inside the glove box to discharge the CR Mg materials flakes. An amount of 5 g of Mg flakes was charged into a tool steel vial (200 mL capacity) supplied by evico GmbH, Großenhainer Str. 101, 01127 Dresden, Germany, together with 60 tool steel balls (10 mm in diameter) at a 45:1 ball-to-powder weight ratio. The sealed vial was then evacuated to a pressure of 10^{-3} bar and pressurized with 50 bar of pure (99.999 wt.%) H_2 gas. The vial was then placed on a high-energy ball mill (PM 400) provided by Retsch GmbH, Retsch-Allee 1–5, 42781 Haan, Germany, and operated at a speed of 250 rpm for 100 h.

A separate set of experiments was performed to determine the effect of the CR process on Mg powders produced after 100 h of reactive ball milling (RBM) in the presence of H_2. The powders that became MgH_2 were charged into a stainless steel (SUS304) tube (8 cm diameter and 200 mm length) and then cold-rolled for 100 passes. The as-CR MgH_2 powders were doped with 10 and 15 wt. % of Nb_2O_5 and then RBM under 50 bar of H_2 for 50 h.

2.2. Sample Characterizations

2.2.1. Crystal Structure

X-ray diffraction (XRD) analysis was conducted using a SmartLab-Rigaku XRD (Rigaku Corporation, 3-9-12, Matsubara-cho, Akishima-shi, Tokyo, Japan) equipped with CuKα radiation at a power output of 9 kW. Field emission high-resolution transmission electron microscopy (HRTEM, JOEL-2100F, Otemachi Nomura Bldg. 13F, 2-1-1, Otemachi, Chiyoda, Tokyo, Japan) was used in conjunction with energy dispersive spectroscopy (EDS) using a scanning transmission electron microscope (STEM) from Oxford Instruments (Asylum Research, NanoAnalysis, 25.2 mi, High Wycombe, UK, HP12 3SE) outfitted with a JEOL-2100F. The objective lens of this microscope has a spherical aberration coefficient (Cs) of 0.5 mm, a resolution of 0.19 nm at the point, and a lattice resolution of 0.12 nm at the lattice. The spot sizes produced by nanobeam diffraction (NBD) were 0.5 and 25 nm, respectively.

2.2.2. Thermal Analysis

Shimadzu Thermal Analysis System/TA-60WS (Shimadzu Manufacturing Co., Ltd., 1 Nishinokyo Kuwabaracho, Nakagyo-ku, Kyoto 604-8511, Japan) was used to study the decomposition temperatures of MgH_2 powders using a differential scanning calorimeter (DSC) at a heating rate of 10 °C/min and under 1 bar of He.

2.2.3. Hydrogenation/Dehydrogenation Behaviors

The kinetics of hydrogen absorption/desorption were studied using Sievert's technique utilizing a PCTPro-2000 supplied by Setaram Instrumentation (11, rue de Sainte Assise, F-77240 Seine-Port, France) at hydrogen gas pressures ranging from 200 mbar (for dehydrogenation) to 10 bar (for hydrogenation). Temperatures of 225, 250, 275, and 350 °C were used to analyze the materials.

3. Results and Discussions

3.1. Morphology and Crystal Structure

Figure 2a illustrates the X-ray diffraction (XRD) patterns and field emission high-resolution transmission electron microscopy (FE-HRTEM) images of Mg-rods following various stages of CR (0 to 200 passes). Clear Bragg peaks matching to hcp-Mg were observed in the sample (PDF# 00-004-0770), with no indication of incompatibility with the given values. (Figure 2a). This may be owing to the absence of lattice imperfections in the MS–Mg ribbons. Meanwhile, low-magnification bright field imaging (BFI) of the as-received Mg-rods (0 passes) revealed twin-free grain boundaries with no indication of lattice defects (Figure 2b), which was in good accordance with the XRD pattern exhibited in Figure 2a. Additionally, the Mg-rods at this starting stage of CR contained large uniaxial grains with irregular size, ranging from 600 nm to 2200 nm, as shown in Figure 2b.

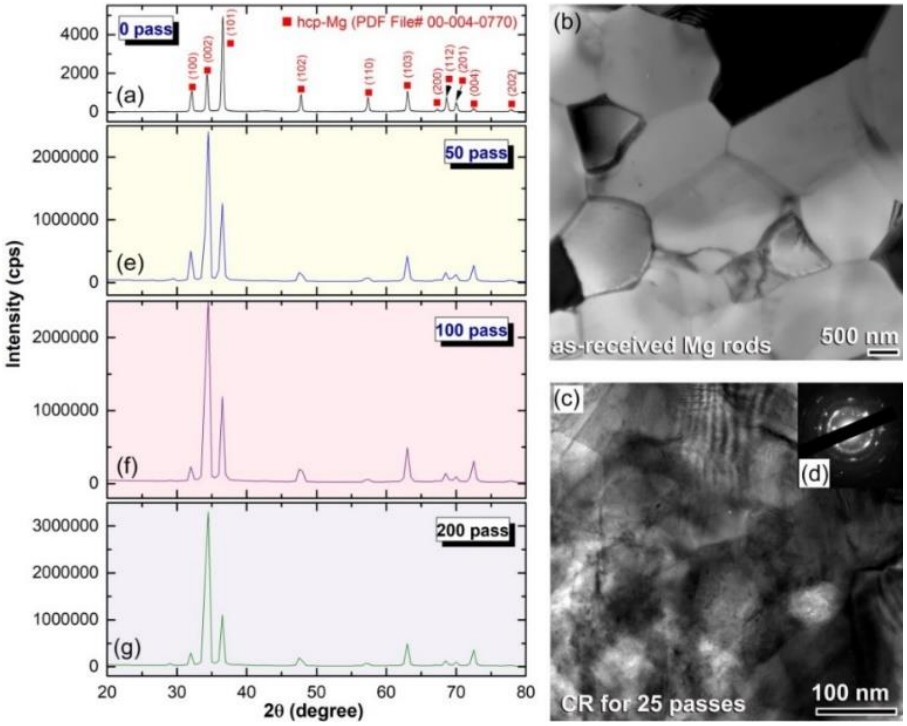

Figure 2. (**a**) XRD pattern and (**b**) the corresponding TEM-BFI of as-received Mg-rods before cold rolling (CR) process. The BFI of the rods obtained after CR for 25 passes is shown together with its related selected area diffraction patterns (SADP) in (**c**) and (**d**), respectively. The XRD patterns of the samples that were CR for 50, 100, and 200 passes are displayed in (**e**), (**f**), and (**g**), respectively.

After 25 cycles of CR, these grains tended to disintegrate along their grain boundaries, forming finer grains (75 nm to 190 nm) of polycrystalline Mg, as presented in Figure 2c,d, respectively. Further CR (50–200 passes) resulted in tremendous lattice defects, as shown by the considerable mismatching of the Bragg peaks for crystallographic planes (002) and (101) in Figure 2e,g. This requires the formation of a high level for the fiber texture's plane (002) [28].

At this stage of CR, Mg grains tended to follow the shear force produced by the process, resulting in plastic deformation (Figure 3b,c) along the CR direction, culminating in elongated Mg grains with apparent sizes between 50 nm to 240 nm, as shown in Figure 3a.

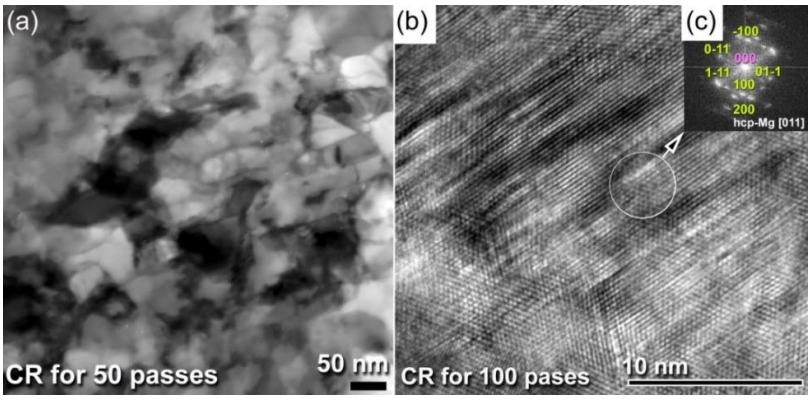

Figure 3. (**a**) BFI of Mg-rods after CR for 50 passes, (**b**) FE-HRTEM image, and (**c**) related scheme 100 passes.

To prepare MgH_2 powders, the snipped Mg flakes obtained after 100 times of CR were high-energy ball-milled under H_2 pressure of 50 bar for 100 h. The FE-HRTEM dark-field image (DFI) and corresponding selected area diffraction pattern (SADP) of the powders obtained after 100 h of RBM are displayed in Figure 4a,b, respectively. The as-RBM powders composited of ultrafine nanocrystalline particles with sizes in the range of 8 nm to 18 nm, as shown in Figure 4a. The SADP of this end-product (100 h) revealed continuous Debye–Scherrer overlapped rings related to tetragonal (β) and orthorhombic (γ)—MgH_2 phases, as indexed in Figure 4b. Formation of MgH_2 powders after 100 h of RBM was also confirmed by XRD (Figure 5a). Figure 5a displays the XRD patterns of CR Mg-flakes for 100 passes after RBM for 100 h.

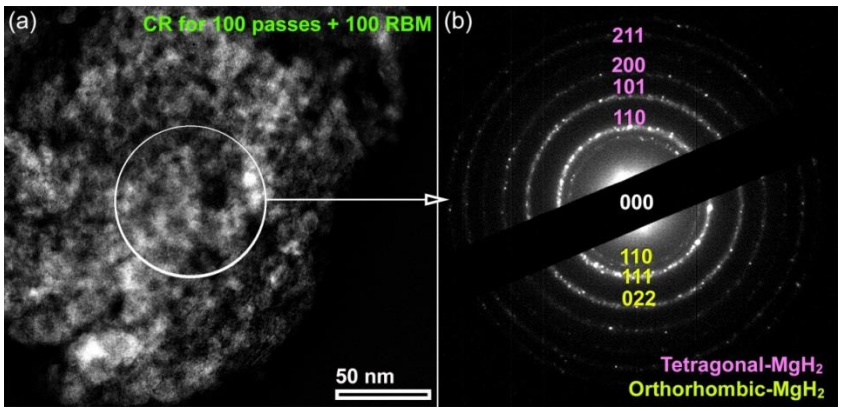

Figure 4. (**a**) DFI of Mg-rods obtained after CR for 100 times followed by 100 h of RBM and (**b**) related SADP.

The formation of the -MgH_2 phase occurred in the presence of minute molecular fractions of the metastable -MgH_2 phase. The lack of Bragg peaks associated with pure hcp-Mg suggests that the RBM process was complete (Figure 5a). The considerable widening of the Bragg peaks observed after 100 h of RBM (Figure 5a) is ascribed to internal strain caused by a high dislocation density and grain refining. Figure 5b illustrates the XRD pattern of Nb_2O_5 powder used as a catalytic agent for MgH_2. The powder exhibited prominent Bragg peaks consistent with the orthorhombic-Nb_2O_5 phase as described (PDF File# 00-027-1003). To increase the hydrogenation/dehydrogenation kinetics and cycle life of MgH_2 produced after 100 h of RBM, 10% and 15% Nb_2O_5 powders were combined and then mechanically ball-milled for 50 h with the metal hydride powders. Figure 5c,d illustrates the XRD patterns of nanocomposite MgH_2/10 wt. percent Nb_2O_5 and MgH_2/15 wt. % Nb_2O_5 powders after 50 h of RBM. Both samples had large Bragg peaks, indicating the creation of nanocrystalline structures.

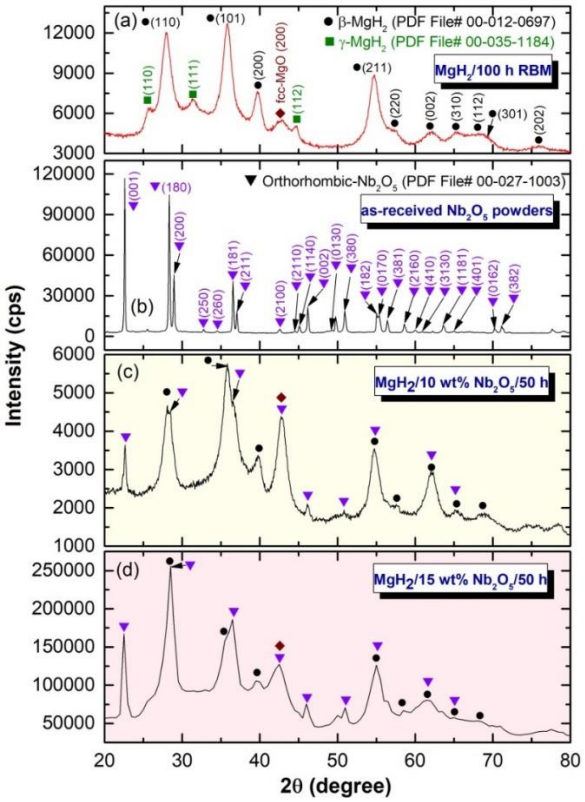

Figure 5. XRD patterns of (**a**) Mg flakes obtained after 100 passes of CR followed by 100 h RBM and (**b**) as-received Nb_2O_5 catalytic powders. The XRD patterns of as-CR MgH_2 after RBM for 100 h and then mechanically ball-milled for 50 h with 10 wt.% and 15 wt.% of Nb_2O_5 are displayed in (**c**) and (**d**), respectively.

FE-HRTEM was utilized to visualize the local structure of the as-RBM nanocomposite powders produced after 50 h of milling. The FE-HRTEM image of MgH_2/10 wt.% Nb_2O_5 is displayed in Figure 6a. The sample after this stage of milling revealed numerous nano-sized grains with different orientations (Figure 6a). Examining the interplanar spacing (d) presented by the Moiré-fringe images indicated that the presence of β- and metastable γ-MgH_2 phases coexisted with orthorhombic-Nb_2O_5, as displayed in Figure 6a. Moreover, the sharp ring SADP pattern shown in Figure 6b, which confirmed the existence of these phases, indicates the formation of nanoscaled grains. This is implied by the lack of sharp spots (Figure 6b).

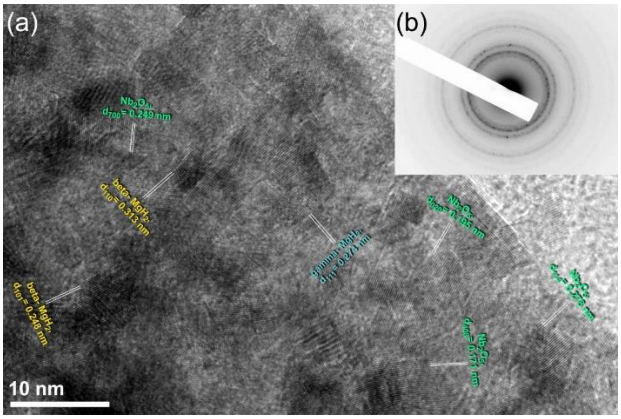

Figure 6. (**a**) FE-HRTEM image and (**b**) corresponding SADP of nanocomposite MgH_2/10 wt.% Nb_2O_5 powders obtained after 50 h of RBM.

3.2. Thermal Stability

The thermal stability of the samples was examined under flow (50 mL/min) of He gas and a heating rate of 10 °C/min. All Mg-rods obtained after different stages of CR process (0–200 passes) were first hydrogenated for 3 h at 350 °C under 50 bar of H_2. The DSC traces of as-received Mg-rods and as-CR samples for 50, 100, and 200 passes are presented collectively in Figure 7a. Each of the thermograms in the figure revealed a single endothermic event associated with the decomposition of the MgH_2 phase. As demonstrated in Figure 6a, the non-CR sample released hydrogen at a relatively high temperature (470 °C). The decomposition temperature (T^{dec}) tended to decrease from 390 °C to 378 °C upon increasing the CR from 50 to 200 passes, respectively, as displayed in Figure 7a. It can be argued that by adding extensive imperfections to the Mg lattice via the CR process, beneficial defects were created at the grain boundaries, resulting in the refinement of the magnesium grains. Due to the formation of such fine grains, the hydrogen diffusion distance was reduced, therefore improving the decomposition kinetics and, hence, reducing the T^{dec} temperature.

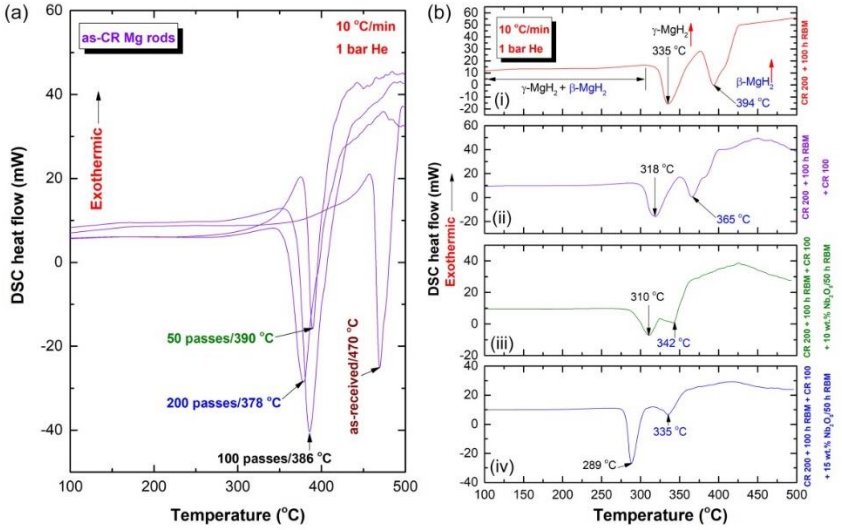

Figure 7. DSC thermograms obtained with 10 °C/min under He atmospheric pressure for (**a**) as-CR Mg rods after processing for 0, 50, 100, and 200 passes and then hydrogenated under 50 bar of H_2 at 400 °C, and (**b**-i) as-200 passes CR Mg obtained after RBM for 100 h, (**b**-ii) as-200 passes +100 h + 100 CR for passes. (**b**-iii) and (**b**-iv) display the DSC curves of the MgH_2 powders catalyzed with 10 wt.% and 15 wt.% of Nb_2O_5 powders, respectively.

In contrast to the CR Mg samples, the thermograms of the sample, which was first CR for 200 passes and then RBM for 100 h, revealed two endothermic events, as displayed in Figure 7b(i). The low-temperature endothermic peak centered at 335 °C was related to the decomposition of metastable γ-MgH_2 phase, where the high-temperature (394 °C) peak corresponded to the decomposition of β-MgH_2 (Figure 7b(i)). The DSC trace of as-CR Mg rods for 200 passes, which were snapped into tiny flakes, and then RBM for 100 h is displayed in Figure 7b(ii). Obviously presented both T^{dec} temperatures related to γ- and β-MgH_2 phases were significantly decreased to 318 °C and 365 °C, respectively (Figure 7b(ii)). This significant deducing in T^{dec} temperatures was attributed to the introduction of further lattice imperfections to the powders that led to the defragmentation of large MgH_2 grains into fine grains. In order to conduct further reduction of the thermal stability for MgH_2 powders, the processed MgH_2 powders were mechanically ball-milled with 10 wt.% (Figure 7b(iii)) and 15 wt.% (Figure 7b(iv)) of Nb_2O_5 powders for 50 h. Doping the metal hydride powders with 10 wt.% Nb_2O_5 led to further decreasing in grain size and this led to further improving in T^{dec} temperatures, which decreased to the level of 310 °C (γ-phase) and 342 °C (β-phase) respectively, as displayed in Figure 7b(iii).

These values of T^{dec} temperatures revealed further decreasing to 289 °C and 335 °C upon mixing with 15 wt.% Nb_2O_5 powders. It has been realized that Nb_2O_5 abrasive powders played the role of micro-milling media, which led to significant reduction in the MgH_2 grain size and hence reduce the T^{dec} temperatures.

3.3. Cycle-Life-Time Performance

The cycle-life-time (CLT) test is the most critical evaluation of the hydrogen storage material since it confirms the material's capabilities to function rapid hydrogenation/dehydrogenation cycles without failure. Figure 8a illustrates the CLT conducted at 350 °C under 10 bar/400 mbar of H_2 for the as-received Mg-rods. Even at a high temperature of 350 °C, the defect-free Mg with its large grain size (Figure 2b) demonstrated extremely sluggish hydrogenation/dehydrogenation rates. This is indicated by the limited number of hydrogenation/dehydrogenation cycles (10 cycles) carried out during a 70 h period. Moreover, this starting material had a very limited capability for hydrogen storage (less than 0.5 wt.% H_2), as shown in Figure 8a. When the Mg-rods were subjected to 200 passes of CR, their hydrogenation/dehydrogenation behavior was improved considerably, as indicated by the increased number of completed absorption/desorption cycles conducted (~90 cycles) at 350 °C under 10 bar/400 mbar of H_2 (Figure 8b). However, its hydrogen storage capacity (~3 wt.% H_2) was still far below the theoretical value of MgH_2 (7.6 wt.% H_2).

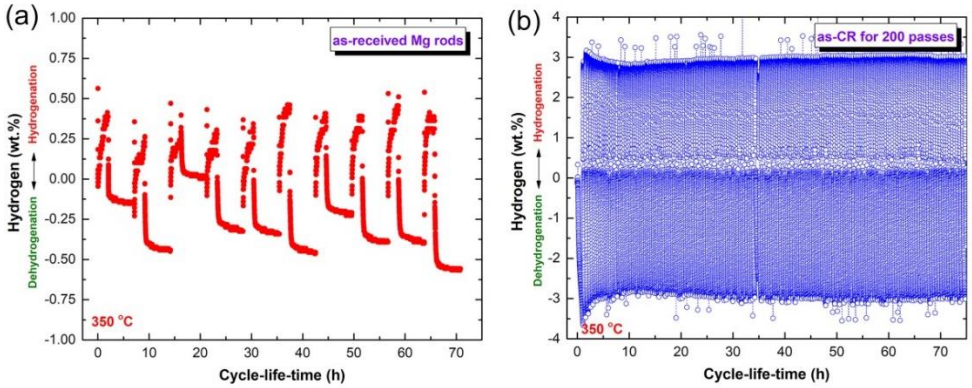

Figure 8. Cycle-life-time (CLT) examined under 10 bar (hydrogenation)/400 mbar (dehydrogenation) of H_2 at 350 °C for Mg-rods obtained after (**a**) 0 passes and (**b**) 200 passes of CR.

When the as-CR Mg rods were snipped into flakes and concurrently RBM for 100 h and then CR for another 100 passes, the CLT performance was significantly improved. Although the CLT of this sample was measured at a lower temperature of 275 °C, it demonstrated a high number of cycles of up to 500 in 600 h without apparent deterioration of the storage capacity, which remained constant at 7.3 weight percent H_2, as shown in Figure 9.

The impact of catalyzed MgH_2 powders with two different Nb_2O_5 concentrations (10 and 15 wt.%) was investigated in the present study. For this set of experiments, the CR-MgH_2 powders produced after 200 passes + 100 h RBM + 100 passes of CR were individually RBM for 50 h with the appropriate Nb_2O_5 concentrations. Figure 9 displays the CLT curve conducted under 10 bar/400 mbar at 225 °C of the catalyzed MgH_2 powders with 10 wt.% Nb_2O_5 obtained after RBM for 50 h. At this low temperature, the sample was able to absorb/desorb ~6.1 wt % of H_2, which remained almost constant (6 wt.% H_2) after processing for ~170 h. Neither degradation in the storage capacity nor retreating in the kinetic of hydrogenation/dehydrogenation could be detected even after the completion of 230 continuous cycles, as displayed in Figure 10a.

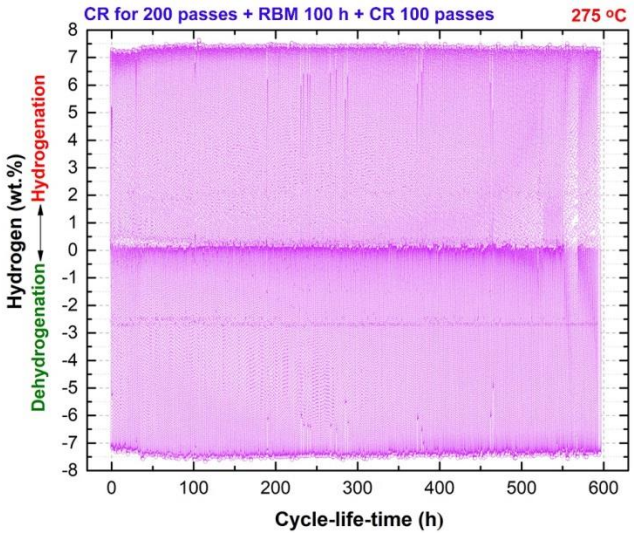

Figure 9. CLT conducted under 10 bar (hydrogenation)/400 mbar (dehydrogenation) of H_2 at 350 °C for Mg-rods obtained after 200 passes. The as-CR rods were then RBM for 100 h and then CR for 100 passes.

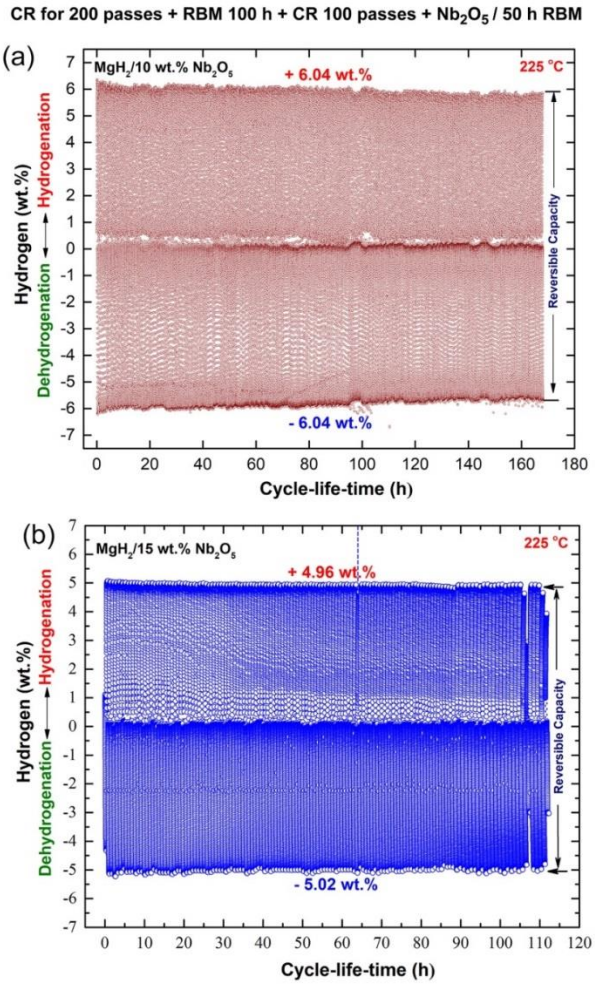

Figure 10. CLT conducted under 10 bar (hydrogenation)/400 mbar (dehydrogenation) of H_2 at 350 °C for Mg-rods obtained after 200 passes. The as-CR rods were RBM for 100 h and then CR for 100 passes. The as-CR powders obtained after 100 passes were individually RBM with Nb_2O_5 powders of (**a**) 10 wt.% and (**b**) 15 wt.%.

The current research demonstrated that the hard Nb_2O_5 nanoparticles functioned well as a nanomilling medium, significantly reducing the particle and grain size of MgH_2. Due to the presence of such fine grains, the hydrogenation/dehydrogenation kinetics in this binary system were improved. Similarly, Simchi et al. [11] observed this result when they ascribed the MgH_2/Nb_2O_5 system's rapid desorption kinetics to grain refining caused by the so-called Nb_2O_5 cracking agent [30]. Due to the well-distributed nature of the hard Nb_2O_5 nanoparticles at the MgH_2 matrix, superior/absorption desorption catalytic effects were produced by these metal oxide powders. According to [31], Nb_2O_5 increases electron exchange reactions with hydrogen molecules, thus initiating the gas–solid reaction. Barkhordarian et al. [10] hypothesized that Nb_2O_5 might also serve as an efficient catalyst for hydrogen recombination, thus accelerating the development of a gas–solid reaction.

The CLT curve for MgH_2 powders doped with 15% Nb_2O_5 after 50 h of RBM is shown in Figure 10b. Excellent hydrogenation properties, as indicated by high cyclic stability even after approximately 110 h (~150 cycles) with no discernible degradation in hydrogen storage capacity, were indicated by nearly constant absorption and desorption values of +4.96 and −5.0 wt.% H_2, respectively, as shown in Figure 10b. It is realized that using a high concentration (15 wt.%) of Nb_2O_5, which has a molecular weight of 265.81 g/mol, led to a significant degradation in MgH_2 storage capacity (~5 wt.%), as indicated in Figure 10b.

4. Conclusions

The present work was conducted in order to investigate the synergetic effect of high-energy reactive ball milling of plastically deformed cold-rolled recycled Mg flakes on hydrogenation/dehydrogenation as well as decomposition processes. For the purpose of this work, the as-received solid waste Mg-rods were firstly cold-rolled 200 times and high-energy ball-milled under an H_2 atmosphere for 100 h. In order to increase the lattice imperfections, the as-ball-milled powders were then cold-rolled for 100 passes and then ball-milled with 10 and 15 wt.% Nb_2O_5 powders for 50 h. As a consequence of being treated to several forms of defects (dislocations, stacking faults, and twining) induced by cold rolling and ball milling, the findings demonstrated that the materials' gas absorption and desorption kinetics were enhanced. When compared with the as-received materials, their capacity to produce a long cycle life at a reduced temperature was used to determine their effectiveness. When treated to RBM with Nb_2O_5 for 50 h, the powders exhibited significant improvement in terms of kinetics and decomposition temperature, indicating that the process was successful. At a relatively moderate temperature (225 °C), the nanocomposite MgH_2/10 and 15 wt.% Nb_2O_5 demonstrated strong hydrogen storage capabilities with a long cycle life that ranged from 110 h to 170 h without a significant decrease in storage capacity and kinetics.

Author Contributions: M.S.E.-E. designed the experimental work, prepared the samples, made the DSC, SEM, and TEM characterizations, shared in kinetics measurements, and wrote the manuscript. N.A. shared in sample preparations, DSC and XRD characterizations and microhardness, and reviewed the manuscript. F.A.-A., M.B., and A.A.A.-D. equally shared in the sample preparations, XRD, DSC, and kinetics measurements. All authors discussed the results and commented on the manuscript and conclusions of this work. All authors have read and agreed to the published version of the manuscript.

Funding: This work has been partially funded by the Kuwait Foundation for the Advancement of Sciences (KFAS) related to Project EA078C under contract number: PR1814SP12.

Institutional Review Board Statement: Not applicable.

Informed Consent Statement: Not applicable.

Data Availability Statement: Not applicable.

Acknowledgments: The financial support received by the Nanotechnology and Advanced Materials Program—Energy and Building Research Center, Kuwait Institute for Scientific Research is highly appreciated.

Conflicts of Interest: The authors declare no conflict of interest.

Sample Availability: Samples of the compounds are not available from the authors.

References

1. Khan, H.; Weili, L.; Khan, I.; Oanh, L.K. Recent advances in energy usage and environmental degradation: Does quality institutions matter? A worldwide evidence. *Energy Rep.* **2021**, *7*, 1091–1103. [CrossRef]
2. El-Eskandarany, M.S. Recent developments in the fabrication, characterization and implementation of MgH_2-based solid-hydrogen materials in the Kuwait Institute for Scientific Research. *RSC Adv.* **2019**, *9*, 9907. [CrossRef] [PubMed]
3. Lee, S.; Kim, T.; Han, G.; Kang, S.; Yood, Y.S.; Jeon, S.Y.; Bae, J. Comparative energetic studies on liquid organic hydrogen carrier: A net energy analysis. *Renew. Sustain. Energy Rev.* **2021**, *150*, 111447. [CrossRef]
4. Hassan, I.A.; Ramadan, H.S.; Saleh, M.A.; Hissel, D. Hydrogen storage technologies for stationary and mobile applications: Review, analysis and perspectives. *Renew. Sustain. Energy Rev.* **2021**, *149*, 111311. [CrossRef]
5. El-Eskandarany, M.S. *Mechanical Alloying: Energy, Surface Protective Coating and Medical Applications*, 3rd ed.; Elsevier: Oxford, UK, 2020.
6. El-Eskandarany, M.S.; Banyan, M.; Al-Ajmi, F. Environmentally friendly nanocrystalline magnesium hydride decorated with metallic glassy zirconium palladium nanopowders for fuel cell applications. *RSC Adv.* **2019**, *9*, 27987. [CrossRef]
7. Wang, Y.; Hao, C.; Ge, Y.; Hao, L.; Tan, J.; Wang, X.; Zhang, P.; Wang, Y.; Tian, W.; Lin, Z.; et al. Fuel consumption and emission performance from light-duty conventional/hybrid-electric vehicles over different cycles and real driving tests. *Fuel* **2020**, *278*, 118340. [CrossRef]
8. Oliveira, A.M.; Beswick, R.R.; Yan, Y. A green hydrogen economy for a renewable energy society. *Curr. Opin. Chem. Eng.* **2021**, *33*, 100701. [CrossRef]
9. El-Eskandarany, M.S.; Banyan, M.; Al-Ajmi, F. Cold-rolled magnesium hydride strips decorated with cold-sprayed Ni powders for solid-state hydrogen storage. *Int. J. Hydrog. Energy* **2019**, *44*, 16852–16861. [CrossRef]
10. Sahlberg, M.; Karlsson, D.; Zlotea, C.; Jansson, U. Superior hydrogen storage in high entropy alloys. *Sci. Rep.* **2016**, *6*, 36770. [CrossRef]
11. Jain, I.P.; Lal, C.; Jain, A. Hydrogen storage in Mg: A most promising material. *Int. J. Hydrog. Energy* **2010**, *35*, 5133–5144. [CrossRef]
12. El-Eskandarany, M.S.; Al-Ajmi, F.; Banyan, M. Mechanically-induced catalyzation of MgH_2 powders with Zr_2Ni-ball milling media. *Catalysts* **2019**, *9*, 382. [CrossRef]
13. El-Eskandarany, M.S.; Shaban, E.; Al-Halaili, B. Nanocrystalline $\beta-\gamma-\beta$ cyclic phase transformation in reacted ball milled MgH_2 powders. *Int. J. Hydrog. Energy* **2014**, *39*, 12727–12740. [CrossRef]
14. El-Eskandarany, M.S.; Al-Matrouk, H.; Shaban, E.; Al-Duweesh, A. Effect of mechanically-induced solid-state doping time on the morphology and hydrogenation cyclability of $MgH_2/7\ Mn_{3.6}Ti_{2.4}$ nanocomposite powders. *Int. J. Hydrog. Energy* **2015**, *40*, 10139–10149. [CrossRef]
15. El-Eskandarany, M.S.; Banyan, M.; Al-Ajmi, F. Discovering a new MgH_2 metastable phase. *RSC Adv.* **2018**, *8*, 32003–32008. [CrossRef] [PubMed]
16. Floriano, R.; Leiva, D.R.; Deledda, S.; Hauback, B.C.; Botta, W.J. MgH_2-based nanocomposites prepared by short-time high energy ball milling followed by cold rolling: A new processing route. *Int. J. Hydrog. Energy* **2014**, *39*, 4404–4413. [CrossRef]
17. Ranjbar, Z.P.; Guo, X.B.; Yu, D.; Wexler, A.; Calka, A.; Kim, C.J.; Liu, H.K. Hydrogen storage properties of MgH_2–SiC composites. *Chem. Phys.* **2009**, *114*, 168–172.
18. El-Eskandarany, M.S.; Alkandary, A.; Aldakheel, F.; Al-Saidi, M.; Al-Ajmi, F.; Banyan, M. Performance and fuel cell applications of reacted ball-milled $MgH_2/5.3$ wt% TiH_2 nanocomposite powders. *RSC Adv.* **2018**, *8*, 38175. [CrossRef]
19. Liang, G.; Huot, J.; Boily, S.; Van, N.A.; Schulz, R. Catalytic effect of transition metals on hydrogen sorption in nanocrystalline ball milled MgH_2–Tm (Tm= Ti, V, Mn, Fe and Ni) systems. *J. Alloys Compd.* **1999**, *292*, 247–252. [CrossRef]
20. Kumar, E.M.; Rajkamal, A.; Thapa, R. Screening based approach and dehydrogenation kinetics for MgH_2: Guide to find suitable dopant using first-principles approach. *Sci. Rep.* **2017**, *7*, 15694. [CrossRef]
21. Xie, L.S.; Li, J.S.; Zhang, T.B.; Kou, H.C. Role of milling time and Ni content on dehydrogenation behavior of MgH_2/Ni composite. *Trans. Nonferrous Metals Soc.* **2017**, *27*, 569–577. [CrossRef]
22. Yu, X.B.; Yang, Z.X.; Liu, H.K.; Grany, D.M.; Walker, G.S. The effect of a Ti-V-based BCC alloy as a catalyst on the hydrogen storage properties of MgH_2. *Int. J. Hydrog. Energy* **2010**, *35*, 6338–6344. [CrossRef]
23. Zhou, C.; Fang, Z.Z.; Ren, C.; Li, J.; Lu, J. Effect of Ti intermetallic catalysts on hydrogen storage properties of magnesium hydride. *J. Phys. Chem. C* **2013**, *117*, 12973–12980. [CrossRef]
24. El-Eskandarany, M.S.; Shaban, E.; Aldakheel, F.; Alkandary, A.; Behbehani, M.; Al-Saidi, M. Synthetic nanocomposite $MgH_2/5$ wt.% $TiMn_2$ powders for solid hydrogen storage tank integrated with PEM fuel cell. *Sci. Rep.* **2017**, *7*, 1. [CrossRef] [PubMed]
25. El-Eskandarany, M.S.; Shaban, E.; Al-Matrouk, H.; Behbehani, M.; Alkandary, A.; Aldakheel, F.; Ali, N.; Ahmed, S.A. Structure, morphology and hydrogen storage kinetics of nanocomposite $MgH_2/10$ wt.% $ZrNi_5$ powders. *Mater. Today Energy* **2017**, *3*, 60–71. [CrossRef]

26. El-Eskandarany, M.S. Metallic glassy $Zr_{70}Ni_{20}Pd_{10}$ powders for improving the hydrogenation/dehydrogenation behavior of MgH_2. *Sci. Rep.* **2016**, *6*, 156. [CrossRef] [PubMed]
27. Amira, S.; Huot, J. Effect of cold rolling on hydrogen sorption properties of die-cast and as-cast magnesium alloys. *J. Alloy. Compd.* **2012**, *520*, 287–294. [CrossRef]
28. Kalisvaart, W.P.; Harrower, C.T.; Haagsma, J.; Zahiri, B.; Luber, E.J.; Ophus, C.; Poirier, E.; Fritzsche, H.; Mitlin, D. Hydrogen storage in binary and ternary Mg-based alloys: A comprehensive experimental study. *Int. J. Hydrog. Energy* **2010**, *35*, 2091–2103. [CrossRef]
29. Chen, J.; Xia, G.; Guo, Z.; Huang, Z.; Liu, H.; Yu, X. Porous Ni Nanofibers with Enhanced Catalytic Effect on the Hydrogen Storage Performance of MgH_2. *J. Mater. Chem. A* **2015**, *3*, 15843–15848. [CrossRef]
30. Ding, X.; Li, Y.; Fang, F.; Sun, D.; Zhang, Q. Hydrogen-induced magnesium–zirconium interfacial coupling: Enabling fast hydrogen sorption at lower temperatures. *J. Mater. Chem. A* **2017**, *5*, 5067–5076. [CrossRef]
31. Chen, Y.; Zhang, H.; Wu, F.; Sun, Z.; Zheng, J.; Zhang, L.; Chen, L. Mn nanoparticles enhanced dehydrogenation and hydrogenation kinetics of MgH_2 for hydrogen storage. *Trans. Nonferrous Met. Soc.* **2021**, *31*, 3469–3477. [CrossRef]
32. El-Eskandarany, M.S.; Al-Nasrallah, E.; Banyan, M.; Al-Ajmi, F. Bulk nanocomposite MgH_2/10 wt.% (8 Nb_2O_5/2 Ni) solid-hydrogen storage system for fuel cell applications. *Int. J. Hydrog. Energy* **2018**, *43*, 23382–23396. [CrossRef]
33. Wang, P.; Wang, A.M.; Zhang, H.F.; Ding, B.Z.; Hu, Z.Q. Hydrogenation characteristics of Mg–TiO_2 (rutile) composite. *J. Alloy. Compd.* **2000**, *313*, 218–223. [CrossRef]
34. Lu, X.; Zhang, L.; Yu, H.; Lu, Z.; He, J.; Zheng, J.; Wu, F.; Chen, L. Achieving superior hydrogen storage properties of MgH_2 by the effect of TiFe and carbon nanotubes. *Chem. Eng. J.* **2021**, *422*, 130101. [CrossRef]
35. Vijay, R.; Sundaresan, R.; Maiya, M.P.; Srinivasa Murthy, S.; Fu, Y.; Klein, H.P.; Groll, M. Characterization of Mg–x wt.% FeTi (x = 5–30) and Mg–40wt.% FeTiMn hydrogen absorbing materials prepared by mechanical alloying. *J. Alloys Compd.* **2004**, *384*, 283–295. [CrossRef]
36. Jorge, A.M.; de Lima, G.F.; Triques, M.R.M.; Botta, W.J.; Langdon, T.G. Correlation between hydrogen storage properties and textures induced in magnesium through ECAP and cold rolling. *Int. J. Hydrog. Energy* **2014**, *39*, 3810–3821. [CrossRef]